**Acknowledgment.** The authors gratefully acknowledge the support of this work by Research Corporation and the Robert A. Welch Foundation. We are also indebted to Dr. D. E. Young of Allied Chemical Corporation for help with the $^{19}F$ nmr spectra and numerous informative discussions.

# Electronic Structure of Oxo-Bridged Iron(III) Dimers

**Harvey J. Schugar,[1] George R. Rossman,[2] Colin G. Barraclough,[3] and Harry B. Gray*[2]**

*Contribution from the Department of Chemistry, Rutgers University, New Brunswick, New Jersey 08903, and No. 4272 from the Arthur Amos Noyes Laboratory of Chemical Physics, California Institute of Technology, Pasadena, California 91109.* *Received June 24, 1971*

**Abstract:** Magnetic susceptibility results and extensive electronic, infrared, and Mössbauer spectral data are presented for $enH_2[(FeHEDTA)_2O]\cdot 6H_2O$, $Na_4[(FeEDTA)_2O]\cdot 12H_2O$, $FeHEDTA\cdot H_2O$, and $NaFeEDTA\cdot 3H_2O$ (HEDTA = *N*-hydroxoethylethylenediaminetriacetate, EDTA = ethylenediaminetetraacetate, and $enH_2^{2+}$ = ethylenediammonium cation). The magnetic and spectral data establish an electronic structural model for the oxo-bridged dimers in which pairs of $S = {}^5/_2$ Fe(III) ions interact antiferromagnetically, with $J \simeq -95\ cm^{-1}$. The oxo-bridged dimers show marked intensity enhancement of the one-center Fe(III) ligand-field bands. There are also several uv bands which are interpreted as arising from simultaneous electronic excitations of Fe(III) pairs. A simple high-spin ligand-field model modified by spin–spin interaction is judged to be considerably more appropriate than the Dunitz–Orgel molecular orbital approach as a vehicle for describing oxo-bridged Fe(III) dimers.

There has recently been considerable interest in oxo-bridged iron(III) dimeric systems. Several complexes of this type have been synthesized and characterized by magnetic susceptibility measurements and Mössbauer spectra.[4–8] Infrared frequencies associated with the oxo-bridging unit have been identified,[4,9] and in certain cases X-ray structures have been obtained.[10–13] Particular importance can be attached to these model complexes in view of the presence of dimeric and polymeric species in the aqueous chemistry of Fe(III) and the probable occurrence of dimeric Fe(III) species in biochemical systems such as the protein hemerythrin.[14] Dimeric ferriporphyrins containing the Fe–O–Fe structural unit have also been characterized.[13,15,16]

In order to formulate a useful electronic structural model for oxo-bridged Fe(III) complexes, we have chosen to study in considerable detail the spectral and magnetic properties of $enH_2[(FeHEDTA)_2O]\cdot 6H_2O$.[17,18] This choice is felicitous because the compound is of known structure[10] and the HEDTA ligand itself does not interfere significantly in the spectral regions of interest. In addition, the closely related complex $Na_4[(FeEDTA)_2O]\cdot 12H_2O$ is available for comparative study, as are the monomers $NaFeEDTA\cdot 3H_2O$ and $FeHEDTA\cdot 1.5H_2O$. The latter complexes provide a reference point for identifying the electronic structural features that are peculiar to the Fe–O–Fe bridging unit.

The present paper reports magnetic and spectroscopic properties over a wide temperature range for $enH_2[(FeHEDTA)_2O]\cdot 6H_2O$ and related compounds. The results are discussed in terms of a ligand-field (LF) model featuring spin–spin interaction of pairs of high-spin Fe(III) ions. This spin–spin-modified ligand-field description is shown to be superior to the Dunitz–Orgel molecular orbital model for these particular oxo-bridged systems.

## Experimental Section

$enH_2[(FeHEDTA)_2O]\cdot 6H_2O$, $Na_4[(FeEDTA)_2O]\cdot 12H_2O$, and $NaFeEDTA\cdot 3H_2O$ were prepared as previously described.[17,19] Solutions of FeHEDTA were prepared by adding 3 equiv of NaOH to solutions of equimolar amounts of ferric chloride and the free ligand.

(1) Rutgers University.
(2) California Institute of Technology.
(3) On leave from the University of Melbourne, Melbourne, Australia.
(4) A. V. Khedekar, J. Lewis, F. E. Mabbs, and H. Weigold, *J. Chem. Soc. A*, 1561 (1967).
(5) A. van den Bergen, K. S. Murray, and B. O. West, *Aust. J. Chem.*, **21**, 1517 (1968).
(6) W. M. Reiff, G. J. Long, and W. A. Baker, Jr., *J. Amer. Chem. Soc.*, **90**, 6347 (1968).
(7) W. M. Reiff, W. A. Baker, Jr., and N. E. Erickson, *ibid.*, **90**, 4794 (1968).
(8) R. R. Berrett, B. W. Fitzsimmons, and A. A. Owusu, *J. Chem. Soc. A*, 1575 (1968).
(9) D. J. Hewkin and W. P. Griffith, *ibid.*, *A*, 474 (1966).
(10) S. J. Lippard, H. J. Schugar, and C. Walling, *Inorg. Chem.*, **6**, 1825 (1967).
(11) (a) M. Gerloch, E. D. McKenzie, and A. D. C. Towl, *J. Chem. Soc. A*, 2850 (1969); (b) P. Coggon, A. T. McPhail, F. E. Mabbs, and V. N. McLachlan, *ibid.*, *A*, 1014 (1971).
(12) E. Fleischer and S. Hawkinson, *J. Amer. Chem. Soc.*, **89**, 720 (1967).
(13) E. B. Fleischer and T. S. Srivastava, *ibid.*, **91**, 2403 (1969).
(14) (a) M. Y. Okamura, I. M. Klotz, C. E. Johnson, M. R. C. Winter, and R. J. P. Williams, *Biochemistry*, **8**, 1951 (1969); (b) J. L. York and A. J. Bearden, *ibid.*, **9**, 4549 (1970); (c) T. H. Moss, C. Moleski, and J. L. York, *ibid.*, **10**, 840 (1971); (d) H. B. Gray, *Advan. Chem. Ser.*, No. 100, 365 (1971); (e) J. W. Dawson, H. B. Gray, H. E. Hoenig, G. R. Rossman, J. M. Schredder, and R.-H. Wang, *Biochemistry*, **11**, 461 (1972).
(15) N. Sadasivan, H. I. Eberspaecher, W. H. Fuchsman, and W. S. Caughey, *ibid.*, **8**, 534 (1969).
(16) I. A. Cohen, *J. Amer. Chem. Soc.*, **91**, 1980 (1969).
(17) H. J. Schugar, C. Walling, R. B. Jones, and H. B. Gray, *ibid.*, **89**, 3712 (1967).
(18) Abbreviations used in this paper include: phen = 1,10-phenanthroline; bipy = 2,2′-bipyridine; terpy = 2,2′,2″-terpyridine; Salen = *N*,*N*′-ethylenebis(salicylideneiminate).
(19) H. J. Schugar, A. T. Hubbard, F. C. Anson, and H. B. Gray, *J. Amer. Chem. Soc.*, **91**, 71 (1969).

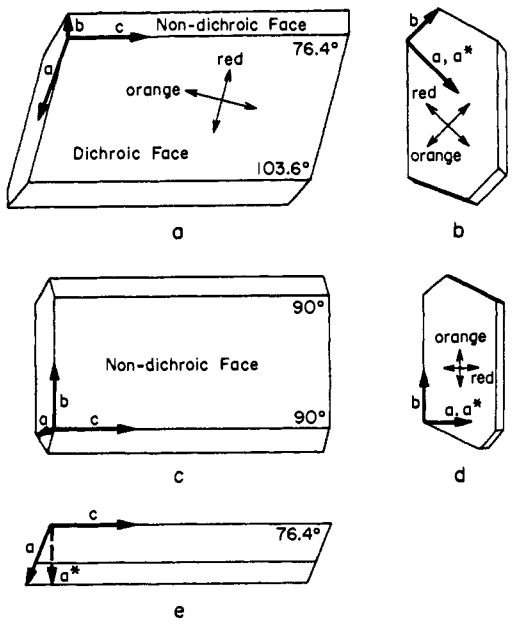


Figure 1. Crystal morphology of $enH_2[(FeHEDTA)_2O]\cdot 6H_2O$. The Fe–O–Fe units are oriented approximately along $a^*$ (perpendicular to bands $b$ and $c$) which coincides with the direction of strongest absorption (red): (a) crystal with developed dichroic face, (b) end view of (a), (c) crystal with developed nondichroic face, (d) end view of (c), (e) side view of (c).

$FeHEDTA\cdot 1.5H_2O$ was obtained from the evaporation of salt-free aqueous solutions of the complex prepared from the reaction of equimolar amounts of ferric hydroxide and free ligand at 80–100° for several minutes. Evaporation of such solutions generally led to the formation of glassy amber films. On occasion, amber crystalline materials could be obtained, and, once in hand, were used to seed additional preparations. *Anal.* Calcd for $C_{10}H_{18}N_2O_{8.5}Fe$: C, 33.54; H, 5.07; N, 7.82; Fe, 15.59. Found: C, 33.90; H, 5.42; N, 7.93; Fe, 15.68.

The above preparative techniques may result in small amounts of finely dispersed hydrous iron oxides being formed or remaining unreacted. For this reason, all solutions of ferric complexes were filtered through 0.22-μm pore size Millipore filters.

The free ligands, $H_3$(HEDTA) and 99.9% reagent grade $Na_2H_2$(EDTA)·$2H_2O$, were used as received from commercial sources. Chemical analyses were performed by Schwarzkopf Microanalytical Laboratory.

The large crystals for single-crystal studies were grown by evaporation at room temperature in still air of aqueous solutions. The crystal morphology of $enH_2[(FeHEDTA)_2O]\cdot 6H_2O$ is shown in Figure 1. The relationship of the unit cell axes to the crystal morphology was determined with oscillation and Weissenberg photographs. Selective development of either the rhomboidal (dichroic) or rectangular (nondichroic) face occurs. As the Fe–O–Fe unit is directed approximately along $a^*$, the electric vector of light normal to the rectangular face always is perpendicular to the Fe–O–Fe direction. The electric vector of polarized light normal to the rhomboidal face can be rotated so as to have substantial components perpendicular (orange) or parallel (red) to the Fe–O–Fe axis. Similar dichroism is also observed for the hexagonal face containing the $a$ axis.

**Spectral Measurements.** All uv, visible, and near-ir spectra were obtained on a Cary 14 RI spectrophotometer. A 1:1 v/v mixture of filtered, saturated aqueous LiCl and water was used for the variable-temperature solution studies.[20] The uv spectra were obtained with the solution held as a thin film between two quartz plates. Visible and near-infrared spectra were obtained in 0.10- and 1.0-cm cells, constructed with rounded edges which minimized the tendency of the glasses to crack at low temperatures.

Polarized spectra were obtained with visible and near-infrared sheet polarizers.

Infrared spectra were taken on a Perkin-Elmer 225 grating spectrophotometer. Solution spectra were taken in 0.05-mm $BaF_2$ cells, using deuterium oxide as a solvent. Solids were handled as KBr and TlBr pellets and Nujol mulls. Low-temperature spectra were taken with a modified Beckman RIIC VLT-2 unit. The samples were run in KBr pellets held in a copper block which fits in the VLT-2. The block temperature was measured with a copper/constantan thermocouple. To minimize heating of the pellets, the source was operated at 75% of normal intensity as measured by the source intensity meter of the instrument.

**Magnetic Susceptibility Measurements.** Magnetic susceptibility measurements were made with a Princeton Applied Research FM-1 vibrating sample magnetometer equipped with an Andonian Associates LHe dewar which allows control of temperature from room temperature down to LHe. Room temperature data were calibrated with $HgCo(SCN)_4$.[21]

For variable-temperature runs, the sample was fitted at the end of a sample rod assembly which contains a copper/constantan thermocouple which fits into the sample holder. The sample temperature was determined by the power in a heater which boils the coolant liquid ($LN_2$ or LHe) and warms the resulting gas which flows by the sample. Variable-temperature data were taken by automatically reducing the power to the heater so that the sample slowly cooled. Magnetometer output (proportional to the susceptibility of the material in the sample region) was continuously plotted *vs.* thermocouple reading on an $X$–$Y$ recorder. The cooling curves were done in two parts. First $LN_2$ was used as a coolant while the sample was cooled from 300 to about 80°K. A second run was later made using LHe as the coolant and covering the range 120°K and lower. The cooling rates—1.75 hr for $LN_2$ and 1.5 hr for LHe—were chosen to be slow enough so that the thermocouple and sample were in thermal equilibrium with each other. The raw data were corrected for the diamagnetism of the sample holder and the effects of the density changes of the gaseous coolant and then calibrated with the room-temperature values of the compounds. The thermocouples were calibrated with $LN_2$, $LH_2$, and LHe; they rapidly lose sensitivity below 30°K. Below 15°K thermometric inaccuracies of 5°K may be possible. The sample volume was 0.33 $cm^3$.

The molar diamagnetic corrections used for $enH_2[(FeHEDTA)_2O]\cdot 6H_2O$ and $Na_4[(FeEDTA)_2O]\cdot 12H_2O$ are $-399\times10^{-6}$ and $-522\times10^{-6}$ cgs, respectively. The molar diamagnetic corrections used for $NaFeEDTA(OH)\cdot 2H_2O$ and for $FeHEDTA\cdot H_2O$ are $-187\times10^{-6}$ and $-157\times10^{-6}$. The respective magnetic moments at 25° are 5.90 and 5.85 BM. These figures were obtained from the measured values of the gram susceptibilities of $H_3$(HEDTA) ($\chi_g = -0.490\times10^{-6}$) and $Na_2H_2$(EDTA)·$2H_2O$ ($\chi_g = -0.475\times10^{-6}$), and from published values for ethylenediamine[22] and Pascal's constants.[23]

**Mössbauer Spectra.** The Mössbauer spectra were obtained by Professor R. H. Herber at Rutgers University. The compounds were finely ground and contained within aluminum foil supports whose spacing was less than 1 mm. The spectrometer and processing of data have been described elsewhere.[24]

## Results and Discussion

**Infrared Spectra.** The infrared spectra of $enH_2[(FeHEDTA)_2O]\cdot 6H_2O$ in KBr and TlBr pellets at 300°K are presented in Figure 2. Equivalent results were obtained with pellets and mineral oil mulls. The band located at 837.5 $cm^{-1}$ is assigned to the antisymmetric stretch of an approximately linear Fe–O–Fe unit.[4,9,25] For this reason, the band has been studied at low temperatures in KBr disks and in $D_2O$ solutions (Figure 3). When a sample of the dimer in a KBr

(20) Aqueous LiCl solutions have proven satisfactory as a glass-forming solvent for use at liquid helium temperatures. Saturated aqueous LiCl and a mixture of two parts saturated LiCl solution and one part water both form clear glasses containing few or no cracks in 1-cm cells when rapidly cooled by immersion into liquid helium. The 1:1 saturated LiCl–$H_2O$ mixture employed in this work formed a crack-free glass when slowly cooled to 25°K.

(21) B. N. Figgis and R. S. Nyholm, *J. Chem. Soc.*, 4190 (1958).

(22) "Handbook of Chemistry and Physics," 46th ed, Chemical Rubber Co., Cleveland, Ohio, 1965, p E-102.

(23) E. König in "Magnetic Properties of Coordination and Organometallic Transition Metal Compounds," Landolt-Börnstein, New Series, Vol. 2, K.-H. Hellwege, Ed., Springer-Verlag, Berlin, 1966, pp 1–18.

(24) R. H. Herber, *Advan. Chem. Ser.*, No. 68, 1 (1967).

(25) R. M. Wing and K. P. Callahan, *Inorg. Chem.*, 8, 871 (1969).

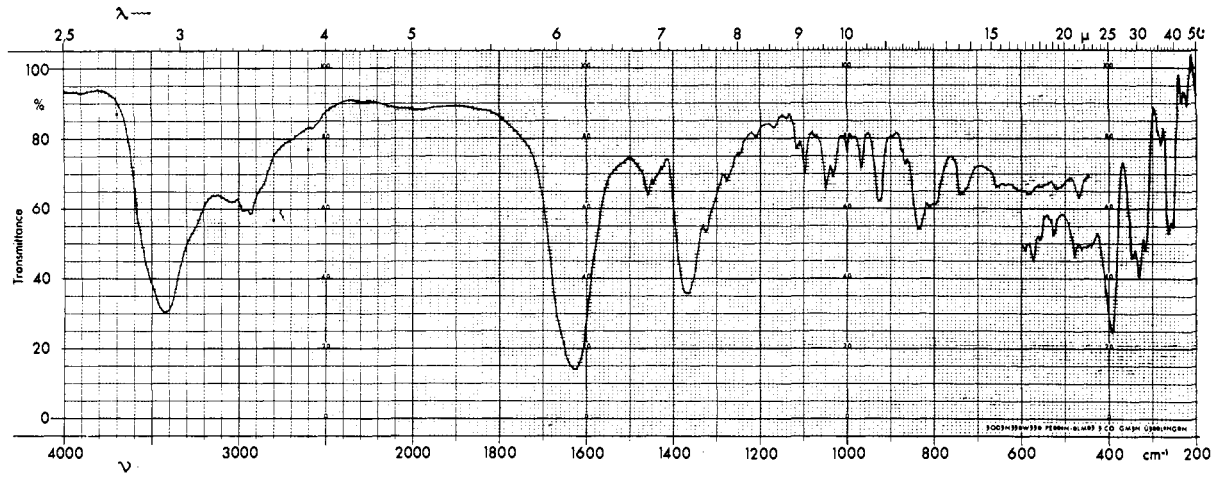


Figure 2. Infrared spectra of $enH_2[(FeHEDTA)_2O]\cdot 6H_2O$; high-energy spectrum, 0.37 mg in 400-mg KBr pellet; low-energy spectrum, 1.44 mg in 400-mg TlBr pellet.

pellet is cooled to 89°K, the Fe–O–Fe band at 837.5 moves to 844.2 $cm^{-1}$. This shift of 6.7 $cm^{-1}$ is larger than typical shifts for ligand bands. (For example, the ligand band at 969.8 $cm^{-1}$ shifts 2.6 $cm^{-1}$ to 972.4 $cm^{-1}$ at 89°K.) The Fe–O–Fe band in the spectrum of $Na_4[(FeEDTA)_2O]\cdot 12H_2O$ at 851.2 $cm^{-1}$ shifts 5.1 $cm^{-1}$ to 856.3 $cm^{-1}$ when the temperature is lowered to 98°K, whereas other bands typically shift 2.3 to 2.5 $cm^{-1}$. The larger blue shift of the Fe–O–Fe band on cooling has also been reported by Reiff, Long, and Baker.[6]

A high-energy shoulder is resolved in solid dimer samples at 867.8 $cm^{-1}$; this shoulder is similar to those observed for other oxo-bridged dimers.[13,16] In the case of the μ-oxo-bis[tetraphenylporphineaquoiron(III)] dimer, the shoulder has also been observed in $CS_2$ solution spectra.[16]

The low-energy ir bands for the Fe–O–Fe dimers, related monomers, and ligands studied here are listed in Table I. A comparison of the absorptions of the monomers and dimers in this region does not reveal any band unique to the dimeric compounds. Thus, we are unable to pinpoint a band attributable to the asymmetric Fe–O–Fe stretching mode, which in several linear M–O–M systems has been reported[25] at ~230 $cm^{-1}$.

**Table I.** Low-Energy Infrared Spectral Data ($cm^{-1}$)

| $Na_4$-[(FeEDTA)$_2$O]·12$H_2O$ | Na-[FeEDTA-(OH$_2$)]·2$H_2O$ | $enH_2$-[(FeHEDTA)$_2$-O]·6$H_2O$ | FeHEDTA-·1.5$H_2O$ |
|---|---|---|---|
| 595 (w)[a] | 578 (m)[a] | 526 (w)[a] | 592 (w)[a] |
| 555 (w, sh) | 511 (w) | 475 (w-m) | 572 (m) |
| 518 (m) | 491 (w) | 439 (w) | 558 (w) |
| 471 (m) | 473 (m) | 407 (w) | 526 (w-m) |
| 440 (w) | 441 (w-m) | 386 (w-m) | 478 (m) |
| 401 (w, sh) | 418 (w, sh) | 367 (w) | 470–430[b] |
| 388 (m-s) | 407 (s) | 341 (m) | 393 (s) |
| 370 (w, sh) | 388 (w) | 311 (w-m) | 345 (m) |
| 313 (s) | 350 (s) | 273 (sh) | 330 (s) |
| 261 (s) | 311 (s) | 260 (s) | 315 (m) |
| | 286 (m-s) | | 282 (w-m) |
| | 262 (s) | | 263 (s) |
| | 221 (m) | | 255 (s) |
| | | | 232 (m) |
| | | | 221 (m) |

[a] w, weak, m, medium; s, strong; sh, shoulder. [b] Several overlapping bands.

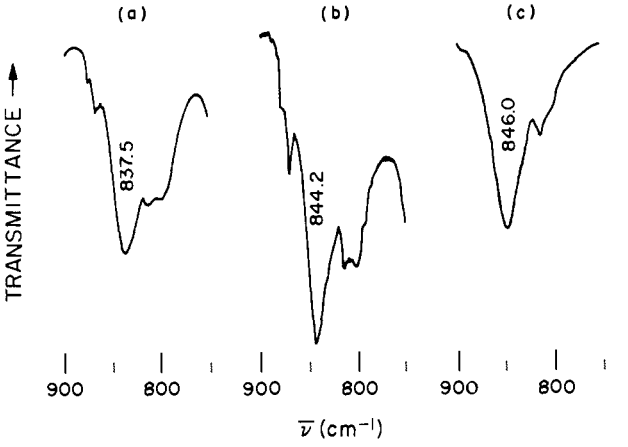


Figure 3. Behavior of the infrared antisymmetric Fe–O–Fe stretch band of $enH_2[(FeHEDTA)_2O]\cdot 6H_2O$: (a) KBr pellet at 310°K, (b) KBr pellet at ~100°K, (c) $D_2O$ solution.

**Magnetic Susceptibility Data.** Magnetic susceptibility results over the temperature range 10–300°K for $enH_2[(FeHEDTA)_2O]\cdot 6H_2O$ and $Na_4[(FeEDTA)_2O]\cdot 12H_2O$ are listed in Table II and presented graphically in Figure 4. The rise in $\chi_g$ at very low temperatures has been observed previously.[6] The data can be fitted by the usual spin–spin interaction model, *i.e.*, taking the Hamiltonian for the interaction as $H = -2JS_1(S_2)$. We have assumed that $S_1 = S_2 = {}^5/_2$, $g = 2.00$, and that $J = -95$ $cm^{-1}$ for $enH_2[(FeHEDTA)_2O]\cdot 6H_2O$ and $J = -99$ $cm^{-1}$ for $Na_4[(FeEDTA)_2O]\cdot 12H_2O$. The theoretical values of $\mu_{eff}$ per Fe(III) shown in Figure 5 are in excellent agreement with the observed $\mu_{eff}$ *vs.* temperature curves.

For each of the above compounds and other related materials containing the Fe–O–Fe structural unit, it is found that the available magnetic data can be fitted equally well with either the $S = ({}^5/_2, {}^5/_2)$ or $S = ({}^3/_2, {}^3/_2)$ models. In no case has a $S = ({}^1/_2, {}^1/_2)$ treatment proved satisfactory.[6,26] The reason that magnetic susceptibility measurements on these systems ($J \cong -100$

(26) J. Lewis, F. E. Mabbs, and A. Richards, *J. Chem. Soc. A*, 1014 (1967).

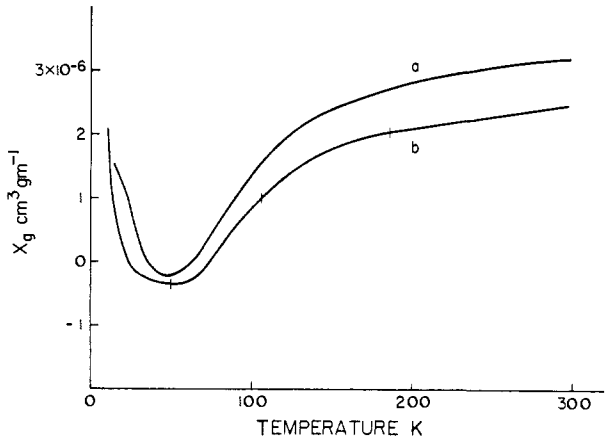


Figure 4. Gram susceptibilities of oxo-bridged dimers as a function of temperature: (a) $enH_2[(FeHEDTA)_2O]\cdot 6H_2O$, (b) $Na_4[(FeEDTA)_2O]\cdot 12H_2O$.

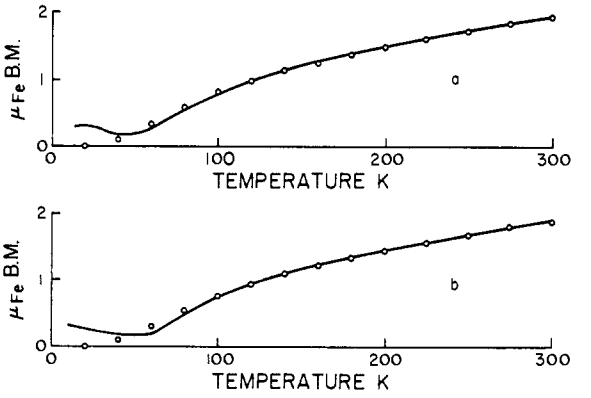


Figure 5. Comparison of the measured (line) and calculated (points) temperature dependence of the magnetic moment per ferric ion of oxo-bridged iron dimers: (a) $enH_2[(FeHEDTA)_2O]\cdot 6H_2O$, $S = (5/2, 5/2)$, $g = 2.0$, $J = -95$ cm$^{-1}$, TIP = 0; (b) $Na_4[(FeEDTA)_2O]\cdot 12H_2O$, $S = (5/2, 5/2)$, $g = 2.0$, $J = -99$ cm$^{-1}$, TIP = 0.

cm$^{-1}$) have been unable to provide a basis for choosing between $S = (5/2, 5/2)$ and $S = (3/2, 3/2)$ is that the additional spin levels of the former case are not appreciably populated below 300°K. Electronic spectra of the two oxo-bridged Fe(III) dimers under consideration here, however, clearly show that the $S = (5/2, 5/2)$ model is the correct choice (*vide infra*). We suggest that this conclusion also applies to the Fe–O–Fe systems that contain phen, bipy, and Salen as nonbridging ligands. Although most of the ligand-field bands are obscured by intense intraligand and charge-transfer absorption, a broad, weak ($\epsilon \sim 3$–7) band is observed[7] in these compounds at about 10,000 cm$^{-1}$ and probably corresponds to the first LF band in $(FeHEDTA)_2O^{2-}$. While two of these other dimers contain five- and seven-coordinate Fe(III), the Fe–O–Fe unit apparently dominates their magnetic behavior; the observed similarities in the magnetic data are probably not accidental.

Esr[27] and anisotropic magnetic susceptibility[11b] measurements support our use of $g = 2.00$ (a value consistent with $^6A_1$ ferric ions). Our calculated results also assume the absence of temperature independent paramagnetism (TIP). The lowest observed susceptibility is $\chi_m = 130 \times 10^{-6}$ cgs unit, which fixes the upper limit for the TIP. Similar upper limits for the TIP have been obtained by others.[6,26]

The spin–spin interaction probably occurs by superexchange through the bridging oxide ion, as the two Fe(III) atoms are too far apart for direct overlap of their d-orbital wave functions. In fact, the oxo-bridged Fe(III) dimers correspond almost exactly to the model situation discussed by Owen and Thornley[28] in their review of the Anderson mechanism of superexchange. They considered two $d^5$ cations with a bridging oxygen anion, the three atoms being in a linear arrangement. It was shown that $J$ should be negative and of the order of magnitude that we observe.

**Table II.** Magnetic Susceptibility Data and Calculated Magnetic Moment per Ferric Ion for $enH_2[(FeHEDTA)_2O]\cdot 6H_2O$ and $Na_4[(FeEDTA)_2O]\cdot 12H_2O$

| | $enH_2[(FeHEDTA)_2O]\cdot 6H_2O$ | | $Na_4[(FeEDTA)_2O]\cdot 12H_2O$ | |
|---|---|---|---|---|
| Temp, °K | $10^6\chi_g$, cm$^3$ g$^{-1}$ | $\mu$, BM | $10^6\chi_g$, cm$^3$ g$^{-1}$ | $\mu$, BM |
| 10 | | | 2.14 | 0.33 |
| 14 | 1.55 | 0.31 | | |
| 26.5 | 0.713 | 0.33 | 0.19 | 0.27 |
| 39.5 | −0.110 | 0.22 | −0.29 | 0.19 |
| 49.5 | −0.210 | 0.21 | −0.30 | 0.21 |
| 58.5 | −0.104 | 0.27 | −0.40 | 0.17 |
| 73.0 | 0.347 | 0.45 | −0.06 | 0.37 |
| 96.1 | 1.29 | 0.76 | 0.70 | 0.69 |
| 115 | 1.77 | 0.93 | 1.30 | 0.92 |
| 149 | 2.38 | 1.20 | 1.73 | 1.16 |
| 186 | 2.73 | 1.42 | 1.97 | 1.37 |
| 235 | 3.00 | 1.67 | 2.22 | 1.61 |
| 257 | 3.10 | 1.76 | 2.31 | 1.72 |
| 288 | 3.16 | 1.88 | 2.43 | 1.85 |
| 297.3 | 3.194 | 1.92 | | |
| 299.7 | | | 2.46 | 1.90 |

**Mössbauer Data.** Mössbauer spectra were measured at 295 and 77°K for $enH_2[(FeHEDTA)_2O]\cdot 6H_2O$, $Na_4[(FeEDTA)_2O]\cdot 12H_2O$, $NaFeEDTA\cdot 3H_2O$, and $FeHEDTA\cdot 1.5H_2O$. The results are compared in Table III with data on two other pairs of oxobridged ferric dimers and corresponding high-spin monomers.

**Table III.** Mossbauer Parameters of Selected Pairs of Monomers and Oxo-Bridged Dimers[a]

| | Isomer shift ($\delta$) | | Quadrupole splitting | |
|---|---|---|---|---|
| Compound | 295°K | 77°K | 295°K | 77°K |
| $enH_2[(FeHEDTA)_2O]\cdot 6H_2O$[b] | 0.63 | 0.74 | 1.69 | 1.75 |
| $FeHEDTA\cdot 1.5H_2O$ | 0.68 | 0.69 | 0.80 | 0.83 |
| $Na_4[(FeEDTA)_2O]\cdot 12H_2O$ | 0.66 | 0.70 | 1.82 | 1.94 |
| $Na[FeEDTA]\cdot 3H_2O$ | 0.66 | 0.73 | 0.75 | 0.76 |
| $[(Fe(terpy))_2O](NO_3)_4\cdot H_2O$ | 0.79 | 0.94 | 1.93 | 2.35 |
| $Fe(terpy)Cl_3$ | 0.69 | 0.81 | 0.54 | 0.54 |
| $(FeSalen)_2O\cdot 2py$ | 0.71 | 0.79 | 0.92 | 0.88 |
| $FeSalenCl\cdot(CH_3NO_2)_x$ | 0.70 | | 1.34 | |

[a] All data expressed in mm/sec relative to a $Na_2Fe(CN)_5NO\cdot 2H_2O$ absorber; 0.35 mm/sec was added to the original isomer shift data for the terpy and Salen complexes which were measured relative to iron foil.[6,7] [b] At 298°K, values of 0.75 and 1.63 mm/sec for $\delta$ and $\Delta E_Q$ were found by Okamura, *et al.*[14a]

Regarding the structural relationships of the compounds reported here, $(FeHEDTA)_2O^{2-}$ and $(FeEDTA)_2O^{4-}$ display nearly identical optical spectra and

(27) M. Y. Okamura and B. M. Hoffman, *J. Chem. Phys.*, **51**, 3128 (1969).

(28) J. Owen and J. H. M. Thornley, *Rep. Progr. Phys.*, **29**, 675 (1966).

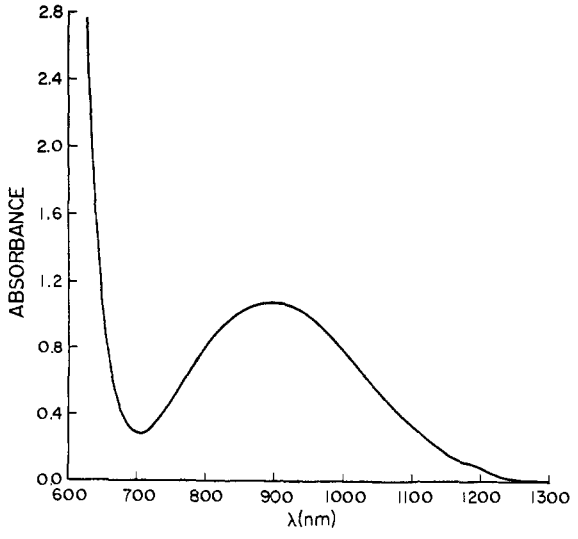


Figure 6. Near-ir spectrum of $enH_2[(FeHEDTA)_2O]\cdot 6H_2O$ at 296°K in saturated LiCl; 0.20 *F*, path 1.0 cm.

presumably have similar coordination environments (distorted octahedral). While the corresponding monomers contain $^6A_1$ ferric ion, seven-coordination has been found in $RbFeEDTA\cdot 3H_2O$[29] and presumably also is present in $NaFeEDTA\cdot 3H_2O$. The detailed structure of $FeHEDTA\cdot 1.5H_2O$ is unknown, and a case can be made for either six- or seven-coordination. The complexes $(FeSalen)_2O\cdot 2py$ and $FeSalenCl\cdot(CH_3NO_2)_x$ have both been characterized by single-crystal X-ray diffraction studies.[11a,30] These compounds are a typical Fe–O–Fe antiferromagnet ($J = -90\ cm^{-1}$) and a high-spin complex, respectively. Each compound contains five-coordinate ferric ion located slightly above the base of a distorted square-pyramidal ligand environment. Neither the pyridine nor nitromethane is coordinated to the ferric ion. The terpyridyl complexes $[(Fe(terpy))_2O](NO_3)_4\cdot H_2O$ and $Fe(terpy)Cl_3$ have been studied by Reiff and coworkers.[6] The compounds are, respectively, an antiferromagnet ($J = -105\ cm^{-1}$) and a high-spin complex. Although the former compound most likely contains an Fe–O–Fe structural unit, no additional structural conclusions can be drawn at this time.

All of the compounds listed in Table III are characterized by approximately the same isomer shift (0.78 ± 0.13 mm/sec). It has been stated that isomer shift values in this range unequivocally establish the ferric ions as being in a sextet spin state and rule out a quartet state.[8] Although the isomer shift criterion for $^6A_1$ ferric ion is reasonable, its utility will not be established until more ferric compounds with spin-quartet ground states are synthesized and fully characterized.

Examination of data in Table III reveals that the monomer–dimer pairs display substantial differences in their $\Delta E_Q$ values. However, the $\Delta E_Q$ differences in these systems do not follow a set pattern and thus their electronic structural significance is not at all clear.

**Electronic Absorption Spectra.** A dominant feature of the near-ir spectrum of an aqueous solution of $(FeHEDTA)_2O^{2-}$ is a broad, weak ($\epsilon$ 3) band at 894 nm (Figure 6). In the crystal, the band appears structured

(29) M. D. Lind, M. J. Harmor, T. A. Harmor, and J. L. Hoard, *Inorg. Chem.*, 3, 34 (1964).
(30) M. Gerloch and F. E. Mabbs, *J. Chem. Soc. A*, 1598 (1967).

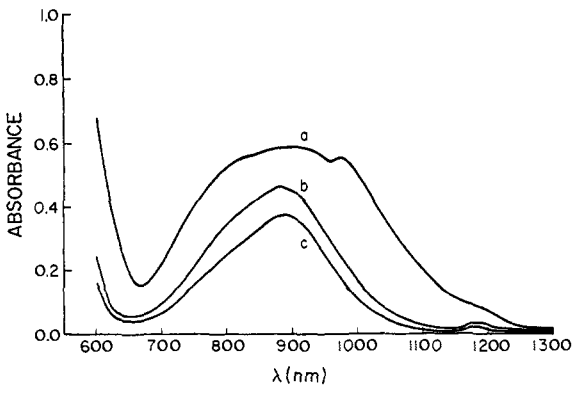


Figure 7. Near-ir spectra of the dichroic (rhomboidal) face of $enH_2[(FeHEDTA)_2O]\cdot 6H_2O$, 0.32-mm thick: (a) 296°K, (b) 89°K, (c) 25°K.

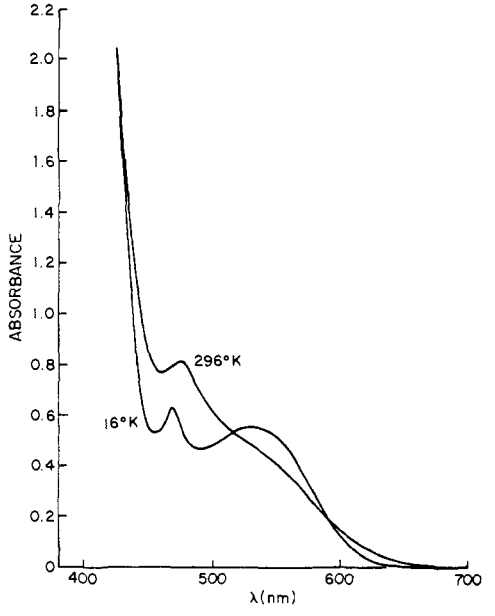


Figure 8. Visible spectra of $enH_2[(FeHEDTA)_2O]\cdot 6H_2O$ at 296 and 16°K in a 1:1 mixture of saturated LiCl and $H_2O$; 0.050 *F*, path 0.1 cm.

and displays the temperature dependence shown in Figure 7. This band (and the $H_2O$ overtone at 971 nm) is strongly polarized along the Fe–O–Fe direction, being almost completely absent in the nondichroic crystal face ($\epsilon$ <0.3).

A search for a lower energy ligand-field absorption band was conducted beyond 1300 nm. As this region cannot be studied in aqueous solution, single crystals were again employed. Two weak bands at 1480 and 1575 nm were observed, but unlike the 894-nm band, they developed the characteristic appearance of vibrational overtones when the crystal was cooled to 25°K. The remainder of the low-energy near-ir consists of vibrational overtone absorptions which display a significant improvement in resolution as the temperature is lowered.

Visible spectra of $(FeHEDTA)_2O^{2-}$ in a 50% saturated LiCl aqueous solution at 296 and 16°K are shown in Figure 8. The spectrum of an aqueous solution at 296°K is essentially the same in the absence of added LiCl. The spectrum at 16°K shows two prominent bands, at 537 and 469 nm. A single-crystal spectrum of

Table IV. Solution Electronic Spectral Data and Band Assignments for $enH_2[(FeHEDTA)_2O]\cdot 6H_2O$

| 296°K[a] | | | Low temperature | | | | |
|---|---|---|---|---|---|---|---|
| λ, nm | $\bar{\nu} \times 10^{-3}$, $cm^{-1}$ | $\epsilon^b$ | λ, nm | $\bar{\nu} \times 10^{-3}$, $cm^{-1}$ | $\epsilon^b$ | Assignment | Calcd sums |
| 894 | 11.2 | 2.6 | *d* | | | $^6A_1 \rightarrow {}^4T_1\ (^4G)$ | |
| 544 | 18.4 | ~40 | 537[d] | 18.6 | ~50 | $^6A_1 \rightarrow {}^4T_2\ (^4G)$ | |
| 477 | 21.0 | ~25 | 469[d] | 21.3 | ~20 | $^6A_1 \rightarrow [{}^4A_1, {}^4E]\ (^4G)$ | |
| (455) | (22.0)[c] | (~2)[c] | | | | | |
| 403 | 24.8 | ~120 | 397[e] | 25.2 | | $^6A_1 \rightarrow {}^4T_2\ (^4D)$ | |
| 343 | 29.2 | | 337[e] | 29.7 | | $[^6A_1 \rightarrow {}^4T_1\ (^4G)] + [^6A_1 \rightarrow {}^4T_2\ (^4G)]$ | 29.6 |
| 307 | 32.6 | | 305[e] | 32.8 | | $[^6A_1 \rightarrow {}^4T_1\ (^4G)] + [^6A_1 \rightarrow {}^4A_1, {}^4E\ [^4G)]$ | 32.2 |
| 273 | 36.6 | | *f* | | | $[^6A_1 \rightarrow {}^4T_2\ (^4G)] + [^6A_1 \rightarrow {}^4T_2\ (^4G)]$ | 36.8 |
| 235 | 42.6 | | 234[e] | 42.7 | | $[^6A_1 \rightarrow {}^4T_2\ (^4G)] + [^6A_1 \rightarrow {}^4T_2\ (^4D)]$ | 43.2 |
| | | | | | | $[^6A_1 \rightarrow {}^4A_1, {}^4E\ (^4G)] + [^6A_1 \rightarrow {}^4A_1, {}^4E\ (^4G)]$ | 4.20 |

[a] 0.20 *F* solution in $H_2O$. [b] ε [per Fe(III)] values were obtained by visually estimating and subtracting out the contributions of overlapping bands. [c] Weak shoulder on the 477-nm band. [d] 0.05 *F* solution in 1:1 saturated LiCl–$H_2O$ at 16°K; infrared overtones in the 900-nm region prevented accurate determination of the 894-nm band position. [e] 0.29 *F* solution in 1:1 saturated LiCl–$H_2O$ at 78°K, thin film. [f] 273-nm band almost completely disappears at low temperatures.

Table V. Electronic Spectral Data and Band Assignments for $Na_4[(FeEDTA)_2O]\cdot 12H_2O$

| $\lambda_{max}$ | $\bar{\nu}$, $cm^{-1} \times 10^{-3}$ | $\epsilon^d$ | Assignment | Calcd sums |
|---|---|---|---|---|
| 888[a] | 11.3 | 3.1 | $^6A_1 \rightarrow {}^4T_1\ (^4G)$ | |
| 543[a] | 18.4 | ~50 | $^6A_1 \rightarrow {}^4T_2\ (^4G)$ | |
| 477[a] | 21.0 | ~35 | $^6A_1 \rightarrow [{}^4A_1, {}^4E]\ (^4G)$ | |
| (464)[a,b] | 21.6 | ~2 | | |
| 405[c] | 24.7 | ~100 | $^6A_1 \rightarrow {}^4T_2\ (^4D)$ | |
| 344[c] | 29.1 | *e* | $[^6A_1 \rightarrow {}^4T_1\ (^4G)] + [^6A_1 \rightarrow {}^4T_2\ (^4G)]$ | 29.7 |
| 309[c] | 32.4 | *e* | $[^6A_1 \rightarrow {}^4T_1\ (^4G)] + [^6A_1 \rightarrow {}^4A_1, {}^4E\ (^4G)]$ | 32.3 |
| 272[c] | 36.8 | *e* | $[^6A_1 \rightarrow {}^4T_2\ (^4G)] + [^6A_1 \rightarrow {}^4T_2\ (^4G)]$ | 36.8 |
| 246[c] | 40.7 | *e* | $[^6A_1 \rightarrow {}^4T_2\ (^4G)] + [^6A_1 \rightarrow {}^4A_1, {}^4E\ (^4G)]$ | 39.4 |
| | | | $[^6A_1 \rightarrow {}^4A_1, {}^4E\ (^4G)] + [^6A_1 \rightarrow {}^4A_1, {}^4E\ (^4G)]$ | 42.0 |

[a] 0.10 *F* solution in 1:1 saturated LiCl–$H_2O$; 296°K. [b] Weak shoulder on the 477-nm band. [c] 0.05 *F* solution in 1:1 saturated LiCl–$H_2O$; 296°K. [d] ε [per Fe(III)] values were corrected for overlapping bands. [e] Strongly overlapping bands; ε values are on the order of $10^3$.

$[enH_2][(FeHEDTA)_2O]\cdot 6H_2O$ also shows two visible absorption bands, at 530 and 475 nm. The band at 530 nm is absent in the nondichroic face, whereas in the dichroic face it is strongly polarized along the Fe–O–Fe direction. The polarization of the 475-nm band is difficult to determine because of interference by both the 530-nm and lower wavelength absorptions. It does not appear to be strongly polarized, however.

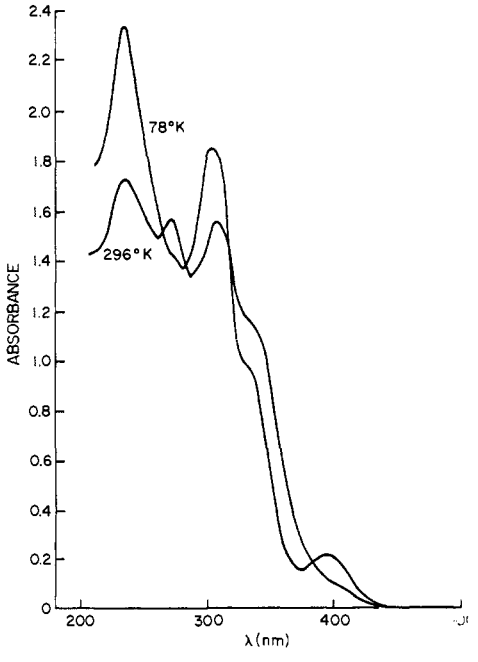


Figure 9. Uv spectra of $enH_2[(FeHEDTA)_2O]\cdot 6H_2O$ at 296 and 78°K in a 1:1 mixture of saturated LiCl and $H_2O$; 0.29 *F*, thin film.

The uv spectrum of $(FeHEDTA)_2O^{2-}$ at 296°K presented in Figure 9 differs in relative band intensity from the previously reported spectrum[19] as a result of using more concentrated solutions in very short path length cells. Under the latter experimental conditions, only a negligible amount of monomeric $[FeHEDTA(OH)]^-$ is present. When cooled to 78°K, the 272-nm band almost completely disappears, and the shoulder near 400 nm develops into a band at 393 nm. The other two uv bands do not undergo large intensity changes at the low temperature.

**Ligand-Field (LF) Bands.** Electronic absorption band positions and transition assignments for $(FeHEDTA)_2O^{2-}$ and $(FeEDTA)_2O^{4-}$ are given in Tables IV and V, respectively. The spectrum of $(FeEDTA)_2O^{4-}$ is essentially the same in all important details as that of $(FeHEDTA)_2O^{2-}$. In both oxo-bridged dimers, the shapes and positions of the first four electronic absorption bands are similar to the LF spectra of typical six-coordinate $^6A_1$ ferric ion complexes[31,32] such as $Fe(H_2O)_6^{3+}$ and $Fe(malonate)_3^{3-}$. (Specifically, we observe two broad bands at low energies followed by a sharper band and a shoulder at higher energies.) The similarity in band positions is reasonable because the relatively weak spin–spin coupling in the dimers is small in comparison to the energies of the d–d transitions (11,000–25,000 $cm^{-1}$). Thus the first four elec-

(31) S. Holt and R. Dingle, *Acta Chem. Scand.*, **22**, 1091 (1968), and references therein.

(32) H. L. Schläfer, *Z. Phys. Chem. (Frankfurt am Main)*, **4**, 116 (1955).

tronic absorption bands of the ferric dimers are assigned as the four lowest LF transitions of an approximately octahedral, high-spin $d^5$ complex ($^6A_1$ ground state): $^6A_1 \rightarrow {}^4T_1$ ($^4G$), $^4T_2$ ($^4G$), [$^4A_1$, $^4E$] ($^4G$), $^4T_2$ ($^4D$). Good agreement with the experimental peak positions for $(FeHEDTA)_2O^{2-}$ is obtained in a LF calculation assuming the parameters $Dq = 1090$, $B = 950$, and $C = 2300\ cm^{-1}$.

The LF spectra of $(FeHEDTA)_2O^{2-}$ and $(FeEDTA)_2O^{4-}$ are surprisingly intense for transitions from $^6A_1$ ground states to quartet excited states. The $^6A_1 \rightarrow {}^4T_1$ ($^4G$) band in $(FeEDTA)_2O^{4-}$, for example, has $\epsilon$ 3.1 (888 nm). The comparable band in a single crystal of $NaFe(EDTA)\cdot 3H_2O$ is at 881 nm, with $\epsilon$ 0.3. Although we have not been able to resolve completely the higher energy LF bands in the high-spin EDTA and HEDTA ferric monomers, it is apparent that they are at least a factor of 10 less intense than the corresponding LF bands in the dimers. It seems reasonable to relate the enhanced intensities to the antiferromagnetic properties of the oxo-bridged Fe(III) dimers, but it is not clear whether removal of simply the parity restriction or relaxation of both parity and spin selection rules is required to account for the observed effect. However, the fact that the band intensities are relatively temperature independent demonstrates that the transitions have acquired considerable orbital allowedness.

Similarly enhanced LF band intensities have been found for a variety of systems containing Mn(II) ions that are bridged by $Cl^-$,[33,34] $F^-$,[35,36] and $S^{2-}$.[37] While such materials contain infinite chains of bridged manganese ions, the nearest-neighbor antiferromagnetic interactions are probably the most important. It was observed that the spin (and parity) "forbidden" Mn(II) LF bands are a factor of 10–50 more intense than those for their magnetically dilute counterparts (*e.g.*, $MnCl_2$ and $MnCl_2\cdot 2H_2O$ *vs.* $MnCl_2\cdot 4H_2O$).

**Simultaneous-Pair Electronic (SPE) Bands.** Each of the two oxo-bridged dimers exhibits four intense uv absorption bands which have been assigned[38] to simultaneous-pair electronic (SPE) transitions. In brief, a single photon simultaneously excites a LF transition on each ferric ion in the Fe–O–Fe unit. In the spin–spin coupling model, the ground- and excited-state dimers have spin manifolds described respectively by $S_{tot} = 5, 4, 3, 2, 1, 0$ and $S_{tot}^* = 3, 2, 1, 0$. Thus, pair transitions which have $S_{tot} = S_{tot}^*$ are fully spin allowed. As the relative oscillator strengths of 0–0 and 1–1 are unknown, we have no way of simply predicting the temperature behavior of the SPE bands.

The spectral data given in Tables IV and V show that the SPE excitation energies correspond closely to sums of the positions of individual ferric ion transitions, as would be expected in the limit of weak spin–spin coupling. Nevertheless, the excellent agreement may be fortuitous, because mixing of SPE excitations with the higher energy, one-center LF transitions could complicate the picture. Additional experimental and theoretical investigations are needed to elucidate more precisely the nature of these unusual electronic absorption bands.

**Reconciliation of Spin–Spin Coupling and Delocalized Molecular Orbital Models for Fe–O–Fe Systems.** We have shown that a model featuring spin–spin coupling of high-spin Fe(III) units satisfactorily accounts for the electronic ground- and excited-state properties of oxo-bridged Fe(III) dimers. An alternative approach based on three-center, delocalized molecular orbitals was first used by Dunitz and Orgel in interpreting the diamagnetic ground states of certain linear M–O–M complexes.[39] Lewis and coworkers have discussed the applicability of the Dunitz–Orgel model to oxo-bridged Fe(III) dimers.[26] Assuming strong $3d\pi$-(Fe)–$2p\pi$(O) bonding, the ground state of an idealized $D_{4h}$ $L_5Fe–O–FeL_5$ system is predicted to be the spin triplet $(e_u)^4(e_g)^4(b_{2g})^2(b_{1u})^2(e_u)^2$. As the known Fe–O–Fe complexes have at best $D_{2h}$ or $C_{2v}$ symmetry, the higher $e_u$ level could be split to give a diamagnetic ground state. However, even if it can be brought into agreement with the experimental magnetic data, the Dunitz–Orgel model is clearly at variance with the observation that the LF spectra of ground-state ($T \leq 30°K$) $(FeHEDTA)_2O^{2-}$ and $(FeEDTA)_2O^{4-}$ demonstrate the presence of $^6A_1$-type ferric ions. For this reason, the spin–spin coupling model is highly preferable as a means of describing the 3d-derived electronic energy levels of Fe–O–Fe systems.

It should be emphasized that the electronic spectral data do not completely rule out $\pi$ bonding. These data simply require that such $\pi$ interaction must involve the empty orbitals of the metal. Thus, in place of strong $2p\pi$–$3d\pi$ bonding we could have $2p\pi$–$4p\pi$ or $2p\pi$–$4d\pi$ interaction. The electronic spectra only show that the 3d energy levels are not significantly perturbed by the formation of the oxo-bridging unit. We stress this point because some type of bonding $\pi$ interaction is strongly indicated by the fact that unusually short M–O distances are invariably found in M–O–M bridging units. In a variety of systems whose structures are accurately known from single-crystal X-ray diffraction studies, the bridging M–O distances are typically 0.1–0.3 Å shorter than reference terminal M–O ($M–OH_2$, M–OH) bond lengths. The bridging Fe–O distance in $(FeHEDTA)_2O^{2-}$, for example, is 1.8 Å, which is 0.2 Å shorter than the sum of the iron and oxygen single-bond radii.[10]

Our suggestion that outer $d\pi$ or $p\pi$ metal orbitals may be utilized in oxo-bridged dimers is also consistent with the fact that nearly all such systems exhibit a strong ir band at about 850 $cm^{-1}$.[25] This survey includes $d^3$, $d^4$, and $d^5$ ions and selections from all three rows in the transition series. The lack of variation in the position of the 850-$cm^{-1}$ band is difficult to accommodate in the Dunitz–Orgel scheme, because $d^3$, $d^4$, and $d^5$ complexes would have different M–O–M bond orders.

A final result of interest is afforded by the structural features of an Al–O–Al system recently studied by Kushi and Fernando.[40] The Al(III) ions are five-coordinate, the ligation of the neutral dimer being completed by four 2-methyl-8-quinolinol anions. A prominent role

(33) L. L. Lohr, Jr., and D. S. McClure, *J. Chem. Phys.*, **49**, 3516 (1968).
(34) C. J. Marzzacco and D. S. McClure, *Faraday Soc. Symp.*, No. 3, 106 (1969).
(35) J. Ferguson, H. J. Guggenheim, and Y. Tanabe, *J. Phys. Soc. Jap.*, **21**, 692 (1966).
(36) J. Ferguson, *Aust. J. Chem.*, **21**, 307 (1968).
(37) D. R. Huffman, *J. Appl. Phys.*, **40**, 1334 (1969).
(38) H. J. Schugar, G. R. Rossman, J. Thibeault, and H. B. Gray, *Chem. Phys. Lett.*, **6**, 26 (1970).
(39) J. D. Dunitz and L. E. Orgel, *J. Chem. Soc.*, 2594 (1953).
(40) Y. Kushi and Q. Fernando, *J. Amer. Chem. Soc.*, **92**, 91 (1970).

for $\pi$ bonding of bridging oxide to the outer $3d\pi$ orbitals of Al(III) is suggested by the unusually short (1.68 Å) Al–O distance.

In summary, the electronic spectral and magnetic properties of the Fe–O–Fe dimers are nicely accommodated by a simple spin–spin coupling model. Extension of this model to include $2p\pi(O)$–$4d\pi$,$4p\pi(Fe)$ interaction allows an interpretation of the Fe–O–Fe bond length and infrared data.

**Acknowledgments.** Research at Rutgers University was supported by the Rutgers Research Council and a Petroleum Research Fund Starter Grant. Research at the California Institute of Technology was supported by the National Science Foundation. The authors wish to thank Professor R. Herber for obtaining the Mössbauer data and Professor J. Potenza for performing the X-ray diffraction studies related to the single-crystal spectral measurements. We are also grateful to Professors R. L. Martin and S. J. Lippard for several stimulating discussions regarding the interpretation of various structural, spectral, and magnetic data for oxo-bridged dimeric complexes.

# Molecular Dynamics of Fluxional Molecules in the Solid State. Cyclooctatetraene–Iron Carbonyl Complexes[1]

**A. J. Campbell, C. A. Fyfe,*[2] and E. Maslowsky, Jr.**

*Contribution from the Department of Chemistry, University of Guelph, Guelph, Ontario, Canada.* *Received August 13, 1971*

**Abstract:** "Wide-line" nmr measurements of the "fluxional" molecules $C_8H_8 \cdot Fe(CO)_3$ and $C_8H_8 \cdot Fe_2(CO)_5$ reveal that the cyclooctatetraene rings possess considerable motional freedom in the solid state, reorienting in their approximate molecular planes, but that the ring in $C_8H_8 \cdot (Fe(CO)_3)_2$ is fixed rigidly in the crystal. The results are discussed with respect to the behavior of the complexes in solution and their bonding.

There has been considerable interest in recent years in the structure and bonding of "fluxional" organometallic molecules.[3] In these molecules the bonding in solution is of a dynamic nature, and the static structure is found only at low temperatures. In this light, the properties of several compounds formed by the reaction of cyclooctatetraene with iron carbonyls[4–14] and with ferric chloride[15,16] have been extensively investigated. Cyclooctatetraene–iron tricarbonyl has been shown to have structure **1** from X-ray measurements,[7] but in solution shows only a single sharp proton resonance at room temperature, due

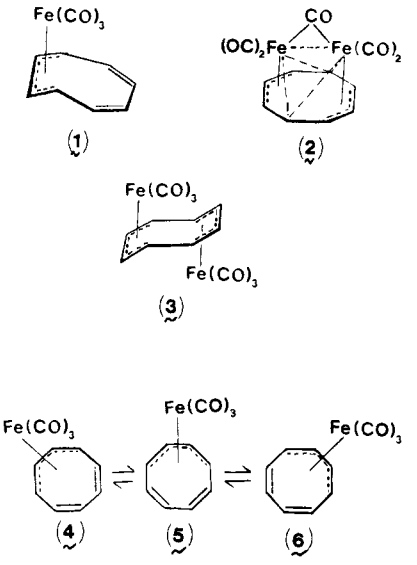


to a rapid equilibrium involving the bonding of the metal atom to the ring. On cooling to $-150°$, a multiplet structure is found.[10–14] There has been some disagreement as to the nature of the rearrangement, due partly to the low-temperature spectrum observed not being the true limiting spectrum. It is now accepted[3] that a 1,2 shift mechanism of the metal atom round the ring as indicated by **4–6** may well be the rearrangement mechanism for *all* cyclooctatetraene–metal tricarbonyls. Similar mobility in the bonding is also found for $C_8H_8 \cdot Fe_2(CO)_5$, known to have structure **2** in the solid state from X-ray diffraction work,[9] but the ring in $(C_8H_8) \cdot (Fe(CO)_3)_2$ (**3**) is found to be quite rigidly bound to the metal atoms.[7]

(1) Preliminary communication: A. J. Campbell, C. A. Fyfe, and E. Maslowsky, Jr., *Chem. Commun.*, 1032 (1971).
(2) Address correspondence to this author.
(3) F. A. Cotton, *Accounts Chem. Res.*, 1, 257 (1968).
(4) T. A. Manuel and F. G. A. Stone, *Proc. Chem. Soc., London*, 90 (1959); *J. Amer. Chem. Soc.*, **82**, 366 (1960).
(5) M. D. Rausch and G. N. Schrauzer, *Chem. Ind. (London)*, 957 (1959).
(6) A. Nakamura and N. Hagihara, *Bull. Chem. Soc. Jap.*, **32**, 880 (1959).
(7) B. Dickens, and W. N. Lipscomb, *J. Chem. Phys.*, **37**, 2084 (1962).
(8) C. E. Keller, G. F. Emerson, and R. Pettit, *J. Amer. Chem. Soc.*, **87**, 1338 (1965).
(9) E. B. Fleischer, A. L. Stone, R. B. K. Dewar, J. D. Wright, C. E. Keller, and R. Petuit, *ibid.*, **88**, 3158 (1966).
(10) C. G. Kreiter, A. Maasbol, F. A. L. Anet, H. D. Kaesz, and S. Winstein, *ibid.*, **88**, 3444 (1966).
(11) F. A. Cotton, A. Davison, and J. W. Faller, *ibid.*, **88**, 4507 (1966).
(12) C. E. Keller, B. A. Shoulders, and R. Pettit, *ibid.*, **88**, 4760 (1966).
(13) F. A. L. Anet, H. D. Kaesz, A. Maasbol, and S. Winstein, *ibid.*, **89**, 2489 (1967).
(14) R. Grubbs, R. Breslow, R. Herber, and S. J. Lippard, *ibid.*, **89**, 6864 (1967).
(15) A. Carbonaro, A. L. Segre, A. Greco, C. Tosi, and G. Dall'Asta, *ibid.*, **90**, 4453 (1968).
(16) G. Allegra, A. Colombo, A. Immirzi, and I. W. Bassi, *ibid.*, **90**, 4455 (1968).